Opto-Electronic Advances

Article

August 2023, Vol. 6, No. 8

DOI: 10.29026/oea.2023.220060

Time-sequential color code division multiplexing holographic display with metasurface

Xin Li[1,2], Qinmiao Chen[3], Xue Zhang[1], Ruizhe Zhao[1], Shumin Xiao[3,4,5]*, Yongtian Wang[1]* and Lingling Huang[1]*

Color metasurface holograms are powerful and versatile platforms for modulating the amplitude, phase, polarization, and other properties of light at multiple operating wavelengths. However, the current color metasurface holography can only realize static manipulation. In this study, we propose and demonstrate a multiplexing metasurface technique combined with multiwavelength code-division multiplexing (CDM) to realize dynamic manipulation. Multicolor code references are utilized to record information within a single metasurface and increase the information capacity and security for anti-cracks. A total of 48 monochrome images consisting of pure color characters and multilevel color video frames were reconstructed in dual polarization channels of the birefringent metasurface to exhibit high information density, and a video was displayed via sequential illumination of the corresponding code patterns to verify the ability of dynamic manipulation. Our approach demonstrates significant application potential in optical data storage, optical encryption, multiwavelength-versatile diffractive optical elements, and stimulated emission depletion microscopy.

Keywords: metasurface; color holography; dynamic display; code division multiplexing

Li X, Chen QM, Zhang X, Zhao RZ, Xiao SM et al. Time-sequential color code division multiplexing holographic display with metasurface. *Opto-Electron Adv* **6**, 220060 (2023).

Introduction

Holography possesses powerful flexible light control and reconstruction abilities, and it has demonstrated significant application value in the acquisition, processing, modulation, storage, and display of optical information. Typically, as a thin hologram, a computer-generated hologram (CGH) without particular optimizations only records the wavefront information for a certain operating wavelength, and a reconstructing beam with different wavelengths leads to a magnification effect[1]. Thus, realization of color computer-generated holography has attracted considerable attention because of its capability to reconstruct different wavefronts at distinct wavelengths. There are two main categories of methods that can be used for realizing color holography: the first type involves the aspect of algorithms, including spatial division methods and depth division methods[2,3], and the other type involves the aspect of systems, which includes

[1]Beijing Engineering Research Center of Mixed Reality and Advanced Display, School of Optics and Photonics, Beijing Institute of Technology, Beijing 100081, China; [2]MoE Key Laboratory of Photoelectronic Imaging Technology and System, and MIIT Key Laboratory of Photonics Information Technology, School of Optics and Photonics, Beijing Institute of Technology, Beijing 100081, China; [3]State Key Laboratory on Tunable Laser Technology, Ministry of Industry and Information Technology Key Lab of Micro-Nano Optoelectronic Information System, Harbin Institute of Technology (Shenzhen), Shenzhen 518055, China; [4]National Key Laboratory of Science and Technology on Advanced Composites in Special Environments, Harbin Institute of Technology, Harbin 150080, China; [5]Collaborative Innovation Center of Extreme Optics, Shanxi University, Taiyuan 030006, China.

*Correspondence: SM Xiao, E-mail: shumin.xiao@hit.edu.cn; YT Wang, E-mail: wyt@bit.edu.cn; LL Huang, E-mail: huanglingling@bit.edu.cn

Received: 1 April 2022; Accepted: 20 June 2022; Published online: 3 November 2022

time division multiplexing (TDM) and spatial division multiplexing (SDM)[4,5]. However, these algorithms lead to multi-order images, which results in low efficiency for the desired color images, and SDM system leads to a setup with a large size, whereas TDM architecture only requires a high performance spatial light modulator (SLM) to realize a compact system. Additionally, as core devices, commercial SLMs have considerable challenges, including a large pixel pitch when compared to the wavelength and strong background noise due to dead zones. An ideal alternative to the current commercial SLM is the use of an optical metasurface.

Metasurfaces consist of subwavelength nanostructure arrays, and they are considered as the next generation of optical elements because of their excellent performance in controlling light properties such as amplitude[6,7], phase[8–10], frequency[11,12], polarization[13,14], and orbital angular momentum[15,16]. Owing to the advantages in subwavelength pixel pitch, ultra-thinness, and multiplexing capabilities, metasurface holography, including optical data storage, information display, and counterfeit protection, has been extensively investigated[17–23]. Multicolor metasurface holography is a significant application with several resolutions. The color CGH algorithms mentioned above are direct methods for realizing color metasurface holography[24,25], where correct images are reconstructed in the region of interest, while multiple orders out of region become background noise. Polarization multiplexing methods can decrease the influence of multiple orders from an algorithm via a linear or circular analyzer[26,27]. Additionally, narrow-band nanostructures consisting of supercells or different color regions on metasurfaces correspond to another common method for color holography[28,29]. In some of these methods, the images are reconstructed in the far field and color printing is realized in white light illumination operating mode[30,31]. A heterogeneous metaatom consisting of both hydrogenated amorphous silicon and gold nanorods was proposed for dual-band holographic reconstruction[32]. And this dual-band holographic operation can also be realized based on a two-layer metasurface[33]. Moreover, harmonic generation is also available to generate bicolor images[34], where C_3 and C_2 nanoantennae are designed for comparable intensities of second-harmonic generation for red and third-harmonic generation for blue. By combining the propagation phase with the geometric phase to generate a phase difference for two wavelengths, another dual-wavelength metasurface holography scheme was realized with wavelength decoupling[35]. Furthermore, building a phase or amplitude library with dispersion is an intuitive strategy for the design of multi-wavelength metasurface[36]. However, above methods only realize static color reconstruction once the devices are fabricated.

Although many efforts have been made to investigate active metasurfaces[37–40], spatiotemporal manipulation is still a challenge. Nevertheless, code division multiplexing (CDM) metasurface holography introduces a new perspective[41]. Inspired by CDM in communications, code references apparently increase the number of manipulation channels and function as tunable illumination assistants for realizing dynamic light modulation. In addition, more channels can be available by introducing other multiplexing methods into metasurface holography because of the compatibility of the CDM. These provide an opportunity to further improve the dynamic modulation potential of color holography.

In this study, we store various images and a color video in a single metasurface by integrating multi-wavelength CDM and polarization multiplexing techniques to enhance the information capacity. Furthermore, a dynamic display is realized with the assistance of a tunable light source and an active optoelectronic modulator. The channel-separated iterative optimization algorithm encodes all the information of the references and targets into CGHs. A titanium dioxide nanorod array was designed and fabricated as a birefringent metasurface. 8 pure color Chinese characters and 8 color video frame images consisting of 48 monochrome images were successfully reconstructed using such a single metasurface, and the video was displayed dynamically with sequential illumination of code reference patterns. Multi-wavelength CDM metasurface holography is an effective scheme for providing extra information channels and vivid colorful holographic videos. It is expected that this method can be employed in high-density optical data storage, optical information encryption, multi-wavelength manipulation, dynamic optical displays, and other fields.

Principle and design

CDM provides an alternative technique to simultaneously allow multiple information manipulations over the same bandwidth[42] in wireless cellular and fiber communication. A series of orthogonal ordered codes are selected as signature waveforms, and they are combined

with target signals and summed before transmission. Then, the receiver decodes her/his signal from the entire information via autocorrelation with the specific code[42]. Essentially, a new information dimension originates from the order of the code signal. Hence, for a free-space two-dimensional (2D) optical information system, similar to a group of specific timing signals selected as codes in communications, a series of well-chosen wavefront distributions can be considered as equivalent candidates to the codes. Specifically, in optical CDM holography, a series of code beams are introduced to encode distinct object information into a single CGH, and these code references are key for decoding the information in reconstruction. The orthogonality of codes is supposed to be obeyed if the concept of CDM from communications is directly applied, which is necessary for communication. Here, because the information for both objects and reconstructed images is mathematically represented by 2D spatial continuum functions, an intuitive definition of orthogonality is defined based on the Hadamard product as follows:

$$\begin{aligned} &E_1(x,y)\circ E_2(x,y)=0 \quad \text{for orthogonal case,}\\ &E_1(x,y)\circ E_2(x,y)\neq 0 \quad \text{for nonorthogonal case ,} \end{aligned} \tag{1}$$

where $\circ$ denotes the Hadamard product of two distributions, $E_1(x,y)$ and $E_2(x,y)$. It is noteworthy that owing to the redundancy property of a hologram that provides a high information density[1], a part of the hologram can be used to record various pieces of information corresponding to distinct reference beams. This indicates that even if there is an overlap between different codes for the non-orthogonal case, the overlapping area of the hologram can still be used to record and reconstruct distinct information successfully when different code beams illuminate the entire CGH. Consequently, orthogonality is not strictly abided by in the implementation of code selection in our CDM method. Then, CDM holography can be described as follows:

$$\begin{aligned} &\left|P\left\{C_n(x,y)\,F\left\{C_m(x,y)\,,t_m(x,y)\right\}\right\}\right|^2\\ &\approx\begin{cases}\left|aP\left\{t_m(x,y)\right\}\right|^2 & m=n\\ \text{noise} & m\neq n\end{cases}, \end{aligned} \tag{2}$$

where $P\{\}$ denotes the propagation of light from the hologram plane to the image plane, $C_m(x,y)$ and $C_n(x,y)$ denote different code beams, $F\{\}$ is an encoding process of CDM holography, $t_m(x,y)$ is the mathematical expression of target object information on the hologram plane, and a represents a complex constant. $t_m(x,y)$ is acquired based on the principle of propagation, which is Fourier transform in our verification for the target image plane locates in spatial frequency domain.

Wavelength can be an independent channel because of the principle of the independent propagation of light in linear materials. Although wavelength division multiplexing (WDM) in optical communications is an effective way for increasing the information capacity by introducing wavelength as another light manipulation dimension, an SDM system consisting of separated sources and modulators for different wavelengths is required. Correspondingly, for CDM holography, it is thought that a strict and precise light manipulation requires orthogonal code beams, where the area occupied for one code pattern cannot be used for another code pattern. Nevertheless, orthogonal codes decrease the flexibility of this method. An alternative method involves independent manipulation of the wavefront at distinct working wavelengths via each modulator unit[42]. Although this is an excellent way to precisely modulate the wavefront, it also increases the difficulty in practical design. For multiwavelength CDM, given that the code references are the main design freedoms, along with the redundancy and robustness properties of holograms, even there are overlapping areas for different color code patterns. Furthermore, the reference beam with the correct color code pattern can read its distinct corresponding optical data and reconstruct the correct wavefront.

The scheme of the multiwavelength CDM metasurface holography is shown in Fig. 1(a). When a given color code beam with specific wavelengths and polarization state illuminates the hologram, the corresponding color holographic image is reconstructed. We utilized 8 code patterns with red, green, and blue (RGB) as the keys and encoded the corresponding color images into the CGH to verify the feasibility of metasurface holography for dynamic multiwavelength manipulation. As shown in Fig. 1(b), 8 pure color patterns with quasi-random color square blocks in a 7×7 matrix were chosen as the code references. The block selection in each code pattern is not completely random because the superimposition of all 8 color patterns should cover the entire metasurface and excessive overlap can result in high-information density. This in turn can lead to the failure of the optical data storage[43]. A total of 54 pure color square blocks (as a group) were selected for 24 monochrome information channels for a specific polarization (8 code channels and 3 color channels). It is worth noting that Fig. 1(d) shows

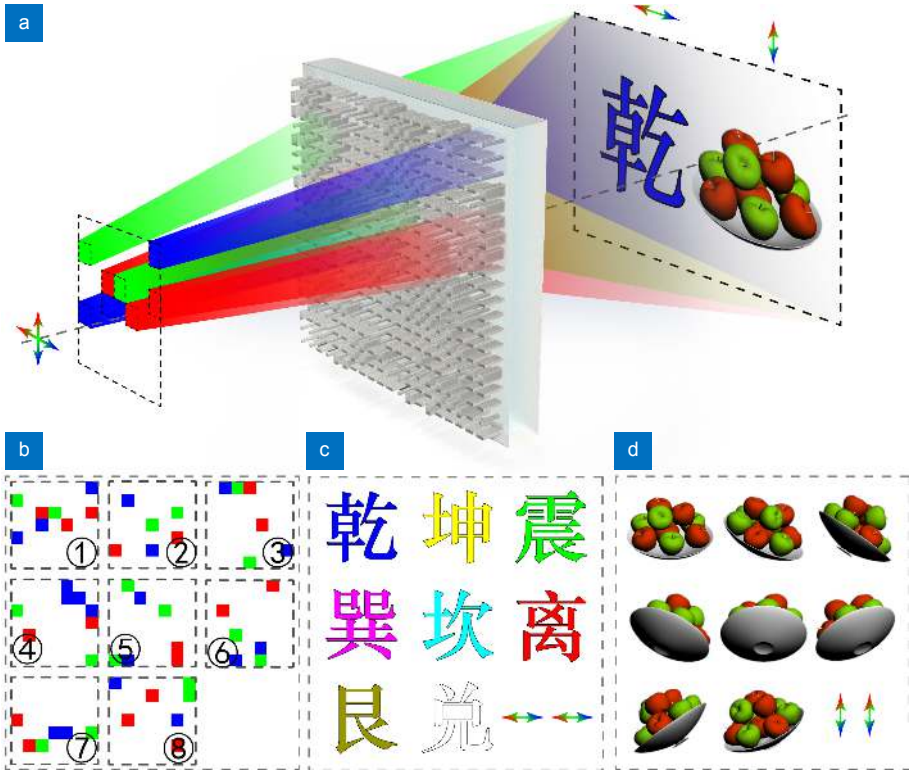

Fig. 1 | (**a**) The schematic of color holographic display based on CDM and polarization multiplexing. The target color image can be reconstructed only when the correct code key reference illuminates on the metasurface with a correct linear polarization state. (**b**) Exhibits eight color code references. (**c**) and (**d**) Color images encoded and recorded for horizontal and vertical polarization channels, respectively.

8 multilevel color images from a color video, and when code patterns from code1 to code8 illuminate the metasurface sequentially with vertical linear polarization, the video is displayed on the observing plane.

The flowchart of three-wavelength CDM hologram encoding process is described in Fig. 2. The color components of all images and codes are separated and encoded into three groups of independent CGHs with RGB colors via a modified Fidoc algorithm respectively. In the encoding process for a specific color channel, all codes and corresponding target images are involved in the iterative optimization process in parallel, and a weighted sum is applied to integrate the information for acquiring a hologram in the current iteration. When the image quality of the reconstructed results satisfies the requirement, the hologram can be outputted as the final CGH for this color channel (for details, please see Supplementary information Section 1). After optimization, they were synthesized as a multiwavelength CDM CGH. Horizontal and vertical linear polarized lights provide another dimension for information storage and reconstruction based on the feature of birefringent metasurfaces, and distinct color images can be encoded or decoded via the exact same code in different polarization channels. Consequently, 16 different color images were recorded in a single metasurface in our verifications.

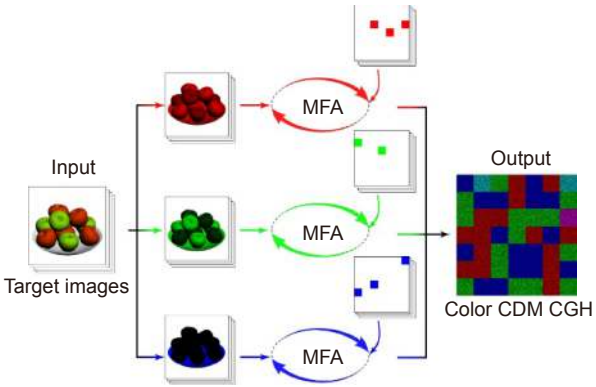

Fig. 2 | Flowchart of optimization algorithm for dynamic multi-wavelength CDM CGHs generation. MFA represents modified Fidoc algorithm for CDM holography according to ref.[41]. The target images are divided into three series of monochromic images for different color components, and they are encoded and synthesized as a multiwavelength CDM CGH.

The metasurface hologram consists of an optimized nanorod array, where the nanorods are composed of titanium dioxide with its high refractive index and low loss in the visible range, and the substrate is composed of silica. In our design, the height of the nanorod was 600

nm, and the period of the unit cell was 360 nm to match the pixel pitch of the image source for the code beams. Considering the complexity and accuracy of nano-fabrication, the length and width of the nanorods were limited to the range of 50 nm to 310 nm. In the simulation and design, a rigorous coupled wave analysis (RCWA) method was applied to analyze the electromagnetic response of the unit cell. The results of the transmission coefficients t_{xx} at 633 nm (R), 532 nm (G), and 460 nm (B) working operating wavelengths are shown in Fig. 3, and the transmission coefficients t_{yy} at each wavelength are symmetrical with t_{xx} via axis rotation. Furthermore, these results form a dictionary for the geometry selection of each nanorod after obtaining color CGH phase profiles. Owing to the robustness of a hologram, each meta-atom, i.e., the unit cell of the metasurface hologram, does not have to offer a precise phase response at each working wavelength. For a specific nanorod, a maximum of 4 channels exist in our verifications (2 color channels due to the selection of code references and two polarization channels as shown in Fig. 1). The optimization function for the size of nanostructures is defined as follows:

$$L = \min\left\{\sum_{\Omega}\left[\left|t_{xx} - \exp\left(\mathrm{i}\varphi_x\right)\right| + \left|t_{yy} - \exp\left(\mathrm{i}\varphi_y\right)\right|\right]\Big|_{\Omega}\right\}, \tag{3}$$

where $\exp\left(\mathrm{i}\varphi_x\right)$ and $\exp\left(\mathrm{i}\varphi_y\right)$ are target CDM CGHs for two polarization channels, and Ω represents the color channel (for instance, the nanorods located in the overlapping area for code1-code8 should be optimized for G and B). Then, the length and width of the nanorods were determined from the transmission coefficient dictionary to ensure that Eq. (3) was minimized.

Results and discussion

We fabricated metasurface samples for experimental verifications. Furthermore, their scanning electronic microscopic images are shown in Fig. 4(a) and 4(b). In addition, Fig. 4(c) exhibits the experiment setup. The nanorod array had 1323×1323 units with an aperture of 476.28 μm×476.28 μm. The light emitted from a supercontinuum laser source is collimated by a spatial filtering system consisting of an objective, pinhole, and lens. The code patterns are loaded on a digital micro-mirror device (DMD) and illuminated on the metasurface sample, where another 4f architecture is employed to filter out diffraction noise via the pixelated structure of the

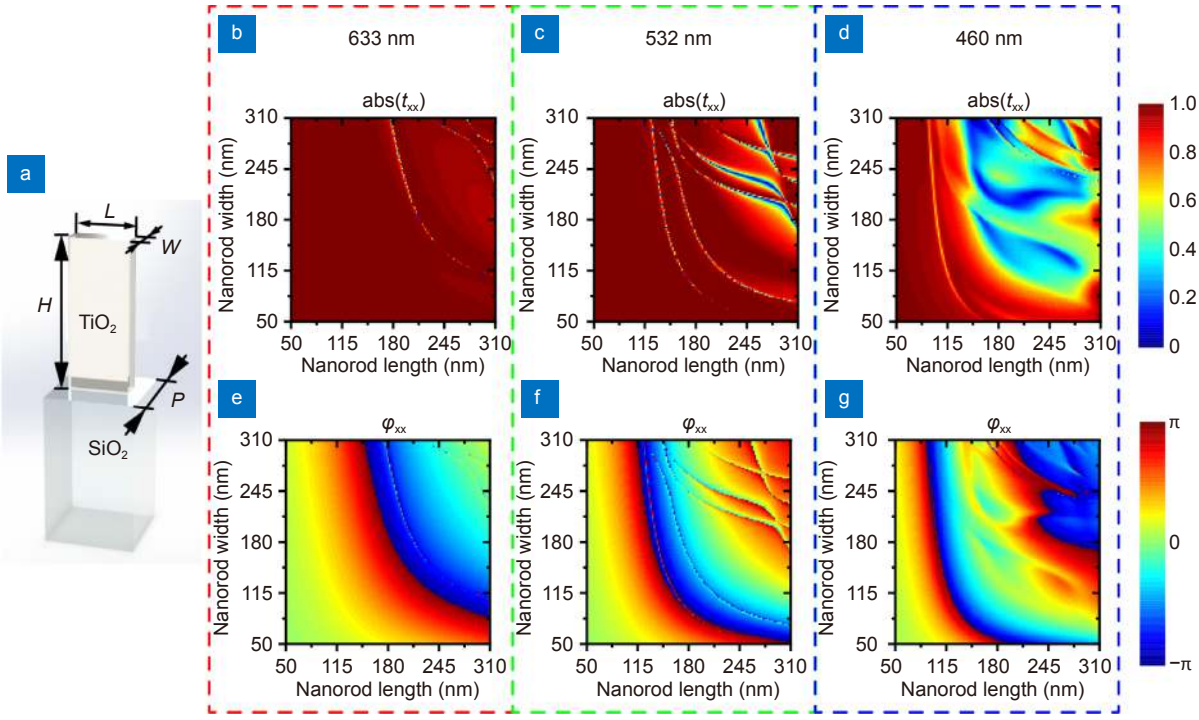

Fig. 3 | (**a**) Schematic illustration of a titanium dioxide nanorod fabricated on a glass substrate, where *H* represents the height (600 nm for the samples), *P* denotes the period of a unit cell (360 nm in our verification), and *W* and *L* are the width and length of nanorods, respectively, whose ranges are from 50 nm to 310 nm. (**b–g**) The simulation scanning results obtained via RCWA for parameters optimizations involving incident wavelengths of 633 nm, 532 nm, and 460 nm. (b–d) and (e–g) are amplitude and phase transmission coefficients t_{xx} of nanorods, respectively.

DMD. Then, the light emitted from the metasurface is collected by an objective and imaged on a camera. A half-wave plate was used to control the polarization state of the incident beam, and an analyzer was utilized to filter out the desired linear polarized light. As shown in Fig. 4, a single DMD is applied for code generation and TDM technique is employed, where R, G, and B lights are emitted sequentially, and the corresponding code patterns are loaded synchronously. Color images are then displayed by combining these three channels due to the persistence of vision.

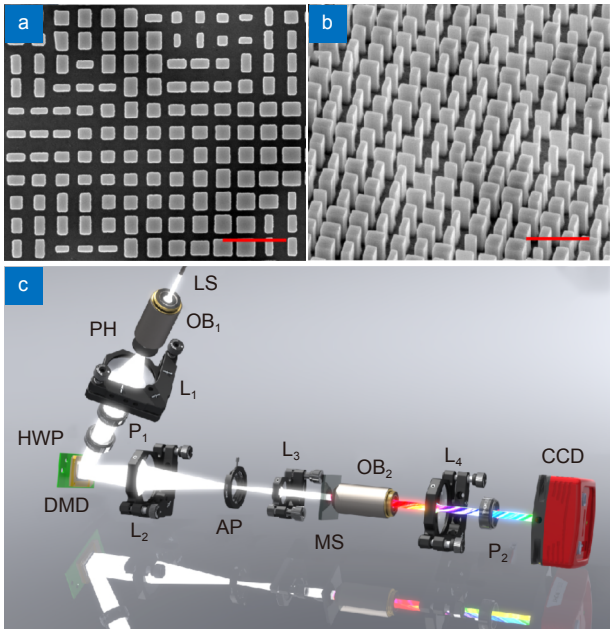

Fig. 4 | (**a**–**b**) Top and oblique views of scanning electron microscopy images of fabricated samples, where the scale bar represents denotes 1 μm. (**c**) Experimental setup. LS, the supercontinuum laser source; OB_1 and OB_2, objective lens; PH, pinhole; L_1–L_4, convex lenses; P_1 and P_2, polarizer and analyzer; HWP, half-wave plate; DMD, digital micro-mirror device; AP, continuously variable iris diaphragm; MS, metasurface; CCD, charge coupled device.

To demonstrate the capabilities of the proposed method, we selected eight Chinese diagrams and frames to form a video as the target images as shown in Fig. 1(b) and 1(c). The reconstructed color images in experiments are shown in Figure 5. Selecting either distinct code patterns or polarization states can offer completely different information channels for a single metasurface. Colorful Chinese characters and multilevel color frame images were successfully reconstructed via code illumination with a specific linear polarization (see Movie S1). It should be noted that bright spots in the center of the results, owing to the unavoidable fabrication errors of the nanorods, the remaining transmitted light from cross-polarization, and slight deviations from the desired transmission coefficient. The strong speckle in the images is attributed to the interference by undesired scattered light, including a slight misalignment between the code illumination and metasurface, and settings of the optical elements in the experiment. Further optimization in the design process and experiments and employment of optical elements with high performance can reduce their influence and bring a higher quality reconstruction. Time sequent illumination of color code patterns leads to the change in reconstructed images. This brings vivid colorful video display (see Movie S1), which indicates that the proposed multiwavelength CDM metasurface holography is an effective way to achieve dynamical manipulating of multiwavelength wavefront.

Multiwavelength CDM metasurface holography is not restricted to the aforementioned three specific wavelengths and limited the number of code references. Additionally, more wavelengths can be realized using the proposed method because the information density provided by the code dimension is sufficiently high. Introducing more wavelength channels and a larger database of codes can further increase the information density of a metasurface, which can be applied to hybrid wavelength-code reference-polarization multiplexing, such as three-dimensional display[44] or hyperspectral light manipulations, with independent wavefronts for each channel. Meanwhile, neither incorrect polarization nor a wrong color code illumination can decode information from the metasurface (see Supplementary information Section 2). Furthermore, time-sequence illumination can provide another key for the correct interpretation of hidden messages. This demonstrates that the multiwavelength CDM metasurface holography has high security, i.e., even if low amount of information is leaked to an eavesdropper, she or he can only decode incorrect information.

There are several multiplexing techniques for metasurface holography based on the variance of the wavefront of incident light such as the point-source method[45] and OAM multiplexing methods[21,46]. However, the information of reference beams in these methods is limited, and many spatiotemporal freedoms are not fully utilized. For the point-source method, the position change of the point source only leads to shifts or magnifications of reconstructed images along the horizontal, vertical, and axial[1], which implies that there is

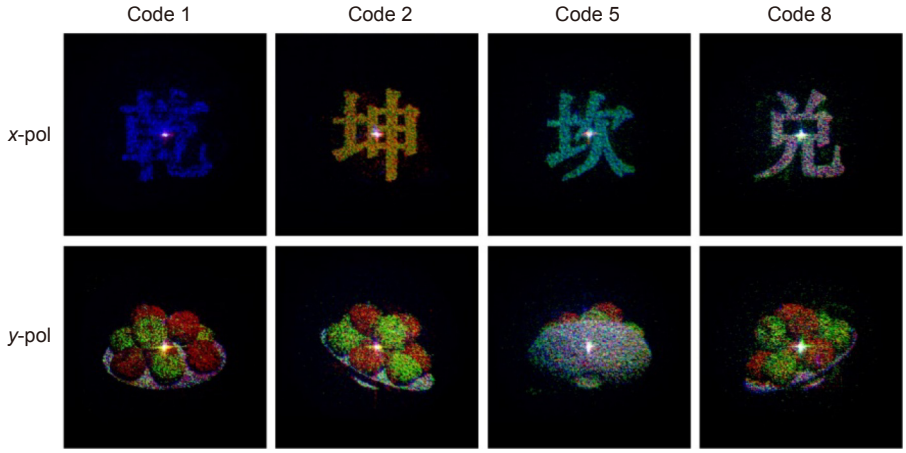

Fig. 5 | Experimental results of multiplexing metasurface holographic color display. The images on the first row are reconstructed with horizontal linear polarization state and four frames from a video with vertical linear polarization are shown on the second row (see Movie S1).

multiorder noise on the observation plane. The topological charge of the vortex beams is the main parameter for multiplex manipulation, which only provides a single extra dimension for light modulation. In CDM metasurface holography, the code patterns are two-dimensional, which results in high information density and flexibility. In addition, CDM metasurface holography has high compatibility, and it works well with other multiplexing light manipulation techniques as shown in our verifications. Accordingly, storing the information of 48 monochrome images is not the upper limit for multiwavelength CDM metasurface holography, and it is easy to realize more states of light manipulation by introducing more multiplexing channels.

The dynamic display is realized owing to the time sequential reading out optical information driven by a DMD. In our verifications, a TDM system is used for color pattern illumination because it is simpler than an SDM system. Moreover, when compared with traditional holographic displays, multiwavelength CDM metasurface holography provides a much higher spatial bandwidth product with a subwavelength pixel pitch. Benefited from this advantage, even a small optical element can record and display an entire color holographic video, which enables the realization of a compact system and has huge potential for practical applications.

Conclusions

A multiwavelength CDM metasurface is introduced to achieve dynamic color holography under the external excitation of color code references with DMD. This type of optical CDM introduces a new manipulation dimension, which enables the recording of high-intensity optical information in a single metasurface via the combination of our improved iterative algorithm and elaborately optimized design of metaatoms. We reconstructed a total of 8 distinct color Chinese characters and displayed a short color video from two polarization channels via the same metasurface hologram, where 48 grey-level monochrome images were stored and read out successfully. Although a TDM illumination system was employed in our verification, simultaneous wavefront manipulation at each working wavelength can be realized by an SDM architecture. This technique demonstrates high compatibility with other multiplexing methods, which leads to higher flexibility, information density, and security. This method is promising for applications in information display, data storage, optical encryption, and other fields with dynamic or multifunctional light manipulation.

References

1. Ackermann G K, Eichler J. *Holography: A Practical Approach* (WILEY-VCH Verlag GmbH & Co. KGaA, Weinheim, 2007).
2. Xue GL, Liu J, Li X, Jia J, Zhang Z, et al. Multiplexing encoding method for full-color dynamic 3D holographic display. *Opt Express* **22**, 18473–18482 (2014).
3. Zheng HD, Zhou CJ, Shui XH, Yu YJ. Computer-generated full-color phase-only hologram using a multiplane iterative algorithm with dynamic compensation. *Appl Opt* **61**, B262–B270 (2022).
4. Li X, Liu J, Zhao T, Wang YT. Color dynamic holographic display with wide viewing angle by improved complex amplitude modulation. *Opt Express* **26**, 2349–2358 (2018).
5. Jia J, Wang YT, Liu J, Li X, Pan YJ, et al. Reducing the memory usage for effectivecomputer-generated hologram calculation using compressed look-up table in full-color holographic display. *Appl Opt* **52**, 1404–1412 (2013).
6. Li J, Zhang YT, Li JN, Yan X, Liang LJ, et al. Amplitude modulation of anomalously reflected terahertz beams using all-optical

active Pancharatnam–Berry coding metasurfaces. *Nanoscale* **11**, 5746–5753 (2019).
7. Huang K, Liu H, Garcia-Vidal FJ, Hong MH, Luk'yanchuk B, et al. Ultrahigh-capacity non-periodic photon sieves operating in visible light. *Nat Commun* **6**, 7059 (2015).
8. Yu NF, Genevet P, Kats MA, Aieta F, Tetienne JP, et al. Light propagation with phase discontinuities: generalized laws of reflection and refraction. *Science* **334**, 333–337 (2011).
9. Decker M, Staude I, Falkner M, Dominguez J, Neshev DN, et al. High‐efficiency dielectric Huygens' surfaces. *Adv Opt Mater* **3**, 813–820 (2015).
10. Zhu LX, Liu X, Sain B, Wang MY, Schlickriede C, et al. A dielectric metasurface optical chip for the generation of cold atoms. *Sci Adv* **6**, eabb6667 (2020).
11. Sain B, Meier C, Zentgraf T. Nonlinear optics in all-dielectric nanoantennas and metasurfaces: a review. *Adv Photonics* **1**, 024002 (2019).
12. Guo XX, Ding YM, Duan Y, Ni XJ. Nonreciprocal metasurface with space–time phase modulation. *Light Sci Appl* **8**, 123 (2019).
13. Rubin NA, D'Aversa G, Chevalier P, Shi ZJ, Chen WT, et al. Matrix Fourier optics enables a compact full-Stokes polarization camera. *Science* **365**, eaax1839 (2019).
14. Bao YJ, Wen L, Chen Q, Qiu CW, Li BJ. Toward the capacity limit of 2D planar Jones matrix with a single-layer metasurface. *Sci Adv* **7**, eabh0365 (2021).
15. Sroor H, Huang YW, Sephton B, Naidoo D, Vallés A, et al. High-purity orbital angular momentum states from a visible metasurface laser. *Nat Photonics* **14**, 498–503 (2020).
16. Guo XX, Ding YM, Chen X, Duan Y, Ni XJ. Molding free-space light with guided wave–driven metasurfaces. *Sci Adv* **6**, eabb4142 (2020).
17. Kim J, Yang Y, Badloe T, Kim I, Yoon G, et al. Geometric and physical configurations of meta-atoms for advanced metasurface holography. *InfoMat* **3**, 739–754 (2021).
18. Jung C, Kim G, Jeong M, Jang J, Dong ZG, et al. Metasurface-driven optically variable devices. *Chem Rev* **121**, 13013–13050 (2021).
19. Gao H, Fan XH, Xiong W, Hong MH. Recent advances in optical dynamic meta-holography. *Opto-Electron Adv* **4**, 210030 (2021).
20. Zhao RZ, Huang LL, Wang YT. Recent advances in multi-dimensional metasurfaces holographic technologies. *PhotoniX* **1**, 20 (2020).
21. Wen DD, Cadusch JJ, Meng JJ, Crozier KB. Light field on a chip: metasurface-based multicolor holograms. *Adv Photonics* **3**, 024001 (2021).
22. Fang XY, Ren HR, Gu M. Orbital angular momentum holography for high-security encryption. *Nat Photonics* **14**, 102–108 (2020).
23. Kim G, Kim S, Kim H, Lee J, Badloe T, et al. Metasurface-empowered spectral and spatial light modulation for disruptive holographic displays. *Nanoscale* **14**, 4380–4410 (2022).
24. Li X, Chen LW, Li Y, Zhang XH, Pu MB, et al. Multicolor 3D meta-holography by broadband plasmonic modulation. *Sci Adv* **2**, e1601102 (2016).
25. Wan WW, Gao J, Yang XD. Full-color plasmonic metasurface holograms. *ACS Nano* **10**, 10671–10680 (2016).
26. Deng ZL, Jin MK, Ye X, Wang S, Shi T, et al. Full-color complex-amplitude vectorial holograms based on multi-freedom metasurfaces. *Adv Funct Mater* **30**, 1910610 (2020).
27. Hu YQ, Li L, Wang YJ, Meng M, Jin L, et al. Trichromatic and tripolarization-channel holography with noninterleaved dielectric metasurface. *Nano Lett* **20**, 994–1002 (2020).
28. Wang B, Dong FL, Li QT, Yang D, Sun CW, et al. Visible-frequency dielectric metasurfaces for multiwavelength achromatic and highly dispersive holograms. *Nano Lett* **16**, 5235–5240 (2016).
29. Huang YW, Chen WT, Tsai WY, Wu PC, Wang CM, et al. Aluminum plasmonic multicolor meta-hologram. *Nano Lett* **15**, 3122–3127 (2015).
30. Bao YJ, Yu Y, Xu HF, Guo C, Li JT, et al. Full-colour nanoprint-hologram synchronous metasurface with arbitrary hue-saturation-brightness control. *Light Sci Appl* **8**, 95 (2019).
31. Wei QS, Sain B, Wang YT, Reineke B, Li XW, et al. Simultaneous spectral and spatial modulation for color printing and holography using all-dielectric metasurfaces. *Nano Lett* **19**, 8964–8971 (2019).
32. Kim I, Jeong H, Kim J, Yang Y, Lee D, et al. Dual-band operating metaholograms with heterogeneous meta-atoms in the visible and near-infrared. *Adv Opt Mater* **9**, 2100609 (2021).
33. Kim J, Jeon D, Seong J, Badloe T, Jeon N, et al. Photonic encryption platform *via* dual-band vectorial metaholograms in the ultraviolet and visible. *ACS Nano* **16**, 3546–3553 (2022).
34. Frese D, Wei QS, Wang YT, Cinchetti M, Huang LL, et al. Nonlinear bicolor holography using plasmonic metasurfaces. *ACS Photonics* **8**, 1013–1019 (2021).
35. Yoon G, Kim J, Mun J, Lee D, Nam KT, et al. Wavelength-decoupled geometric metasurfaces by arbitrary dispersion control. *Commun Phys* **2**, 129 (2019).
36. Shi ZJ, Khorasaninejad M, Huang YW, Roques-Carmes C, Zhu AY, et al. Single-layer metasurface with controllable multiwavelength functions. *Nano Lett* **18**, 2420–2427 (2018).
37. Shaltout AM, Shalaev VM, Brongersma ML. Spatiotemporal light control with active metasurfaces. *Science* **364**, eaat3100 (2019).
38. Kim J, Seong J, Yang Y, Moon SW, Badloe T, et al. Tunable metasurfaces towards versatile metalenses and metaholograms: a review. *Adv Photonics* **4**, 024001 (2022).
39. Kim I, Kim WS, Kim K, Ansari MA, Mehmood MQ, et al. Holographic metasurface gas sensors for instantaneous visual alarms. *Sci Adv* **7**, eabe9943 (2021).
40. Kim I, Jang J, Kim G, Lee J, Badloe T, et al. Pixelated bifunctional metasurface-driven dynamic vectorial holographic color prints for photonic security platform. *Nat Commun* **12**, 3614 (2021).
41. Li X, Zhao RZ, Wei QS, Geng GZ, Li JJ, et al. Code division multiplexing inspired dynamic metasurface holography. *Adv Funct Mater* **31**, 2103326 (2021).
42. Rao R, Dianat S. *Basics of Code Division Multiple Access (CDMA)* (SPIE, Bellingham, Washington, 2005).
43. Cox IJ, Sheppard CJR. Information capacity and resolution in an optical system. *J Opt Soc Am A* **3**, 1152–1158 (1986).
44. Zhan T, Xiong JH, Zou JY, Wu ST. Multifocal displays: review and prospect. *PhotoniX* **1**, 10 (2020).

45. Bao YJ, Yan JH, Yang XG, Qiu CW, Li BJ. Point-source geometric metasurface holography. *Nano Lett* **21**, 2332–2338 (2021).
46. Ren HR, Fang XY, Jang J, Bürger J, Rho J, et al. Complex-amplitude metasurface-based orbital angular momentum holography in momentum space. *Nat Nanotechnol* **15**, 948–955 (2020).

Acknowledgements

The authors acknowledge the funding provided by the National Key R&D Program of China (2021YFA1401200), Beijing Outstanding Young Scientist Program (BJJWZYJH01201910007022), National Natural Science Foundation of China (No. U21A20140, No. 92050117), and Beijing Municipal Science & Technology Commission, Administrative Commission of Zhongguancun Science Park (No. Z211100004821009). X. Li acknowledges the support from Beijing Institute of Technology Research Fund Program for Young Scholars (XSQD-201904005). The authors also acknowledge the fabrication and measurement service in the Analysis & Testing Center, Beijing Institute of Technology.

Competing interests

The authors declare no competing financial interests.

Supplementary information

Supplementary information for this paper is available at https://doi.org/10.29026/oea.2023.220060